Biogenesis Synthesis of ZnO NPs: Its adsorption and photocatalytic activity for removal of acid black 210 dye

Zahraa A. Najm

Mohammed A. Atiya

Ahmed K. Hassan

University of
Kerbala

Biogenesis Synthesis of ZnO NPs: Its adsorption and photocatalytic activity for removal of acid black 210 dye

Abstract

This study investigated the treatment of textile wastewater contaminated with Acid Black 210 dye (AB210) using zinc oxide nanoparticles (ZnO NPs) through adsorption and photocatalytic techniques. ZnO NPs were synthesized using a green synthesis process involving eucalyptus leaves as reducing and capping agents. The synthesized ZnO NPs were characterized using UV-Vis spectroscopy, SEM, EDAX, XRD, BET, Zeta potential, and FTIR techniques. The BET analysis revealed a specific surface area and total pore volume of 26.318 m^2/g. SEM images confirmed the crystalline and spherical nature of the particles, with a particle size of 73.4 nm. A photoreactor was designed to facilitate the photo-degradation process. The study investigated the influence of key variables on the adsorption and photocatalytic break-down of AB210. The results indicated that under optimal conditions (AB210 concentration: 5 mg/L, ZnO NPs dosage: 0.75 g/L, pH: 5, and temperature: 45 °C), the removal efficiency after 180 minutes of adsorption was 62%. However, in the case of photo-degradation, complete removal of 5 mg/L AB210 was achieved within 30 minutes at a pH of 7, UV intensity of 24 W/m^2, and temperature of 45 °C. The adsorption process exhibited the best fit with the pseudo-second-order kinetic model. Various adsorption isotherms, including Freundlich, Langmuir, Temkin, and Dubinin models, were studied, and the Langmuir isotherm provided the best fit to the experimental data (see Supplementary Materials). Fur-thermore, thermodynamic analysis indicated that the adsorption process was spontaneous, endothermic, and favorable, with ΔG°, ΔH°, and ΔS° values of -0.782 kJ/mol, 26.93 kJ/mol, and 0.086 kJ.mol/K, respectively.

Keywords

Zinc oxide nanoparticles; Adsorption process; Photocatalyst; Green method; Photo-reactor; Kinetic study.

Creative Commons License

RESEARCH PAPER

Biogenesis Synthesis of ZnO NPs: Its adsorption and photocatalytic activity for removal of acid black 210 dye

Zahraa A. Najm [a],*, Mohammed A. Atiya [a], Ahmed K. Hassan [b]

[a] Al-Khwarizmi College of Engineering, University of Baghdad, Baghdad, Iraq
[b] Environment and Water Directorate, Ministry of Science and Technology, Baghdad, Iraq

Abstract

This study investigated the treatment of textile wastewater contaminated with Acid Black 210 dye (AB210) using zinc oxide nanoparticles (ZnO NPs) through adsorption and photocatalytic techniques. ZnO NPs were synthesized using a green synthesis process involving eucalyptus leaves as reducing and capping agents. The synthesized ZnO NPs were characterized using UV−Vis spectroscopy, SEM, EDAX, XRD, BET, Zeta potential, and FTIR techniques. The BET analysis revealed a specific surface area and total pore volume of 26.318 m^2/g. SEM images confirmed the crystalline and spherical nature of the particles, with a particle size of 73.4 nm. A photoreactor was designed to facilitate the photo-degradation process. The study investigated the influence of key variables on the adsorption and photocatalytic breakdown of AB210. The results indicated that under optimal conditions (AB210 concentration: 5 mg/L, ZnO NPs dosage: 0.75 g/L, pH: 5, and temperature: 45 °C), the removal efficiency after 180 min of adsorption was 62%. However, in the case of photo-degradation, complete removal of 5 mg/L AB210 was achieved within 30 min at a pH of 7, UV intensity of 24 W/m^2, and temperature of 45 °C. The adsorption process exhibited the best fit with the pseudo-second-order kinetic model. Various adsorption isotherms, including Freundlich, Langmuir, Temkin, and Dubinin models, were studied, and the Langmuir isotherm provided the best fit to the experimental data (see Supplementary Materials). Furthermore, thermodynamic analysis indicated that the adsorption process was spontaneous, endothermic, and favorable, with $\Delta G°$, $\Delta H°$, and $\Delta S°$ values of −0.782 kJ/mol, 26.93 kJ/mol, and 0.086 kJ mol/K, respectively.

Keywords: Zinc oxide nanoparticles, Adsorption process, Photocatalyst, Green method, Photoreactor, Kinetic study

1. Introduction

Annually a significant quantity of dye materials, approximately 70,000 tons, is manufactured, and a notable portion ranging from 10 to 15 percent is released into the environment [1,2]. Additionally, various industries including textiles, pulp and paper, plastics, and leather, rely extensively on dyes during their production processes, resulting in the generation of wastewater containing these colorants [3,4]. These dyes have been identified as potential carcinogens and pose harmful effects on biological systems. Consequently, it becomes crucial to eliminate these hazardous pollutants from

industrial effluents before they are discharged into ecological systems and natural aquatic environments [5,6]. Various treatment techniques, such as coagulation, flocculation, membrane treatment, ion exchange, and biological techniques, are used to remove dyes from contaminated water. However, it is well known that these dyes are extremely persistent and difficult to eliminate using standard treatment techniques [5,7]. Research has been used to create effective strategies for eliminating these colors. Due to its high efficacy, simplicity of use, and ease of operation, adsorption has been extensively used to treat wastewater containing dye contaminants [8,9]. Basically, the adsorption of the molecules

to the adsorbent surface can occur in two ways: "physical adsorption," also called "physisorption," and "chemical sorption," also called "chemisorption." This depends on the interactions between the molecules and the surface [10,11]. Additionally, advanced oxidation processes (AOPs), which cause the production of hydroxyl free radicals (•OH), are considered promising [12,13].

One of the important AOPs, the photocatalytic process, uses semiconductors like TiO_2 [14], ZnS [15], ZnO [16], MgO, Co_3O_4 [17], and CuO [18] to produce •OH and other reactive oxidizing species. AOPs can eliminate both organic and inorganic pollutants [19,20] AOPs are superior to conventional treatment methods because they don't have a problem with secondary waste material production or removal [21,22]. There are currently methods, such as adsorption, that either concentrate or move the dye molecules in effluent into a diffuse phase [23,24]. Photocatalytic technique is very important for dye degradation, CO_2 reduction, H_2 production, and sterilization [25,26]. The specifications of zinc oxide photocatalyst qualify it to be used effectively in the remediation process. It features wide UV radiation absorption, a large abundance, chemical stability under UV radiation, and is non-toxic [27,28]. The summary of the interaction process is given as follows: When light hits the surface of ZnO, charged electrons from the valence band move into the conduction band (e_{CB}^-). The redox reaction occurs on the photoexcited ZnO surface, and •OH is produced as a result of valence band holes (h_{VB}^+) oxidizing water molecules and hydroxide ions The reactions below summarize the •OH production from ZnO NPs [29].

$$Photocatalyst + hv \rightarrow h_{VB}^+ + e_{CB}^- \qquad (1)$$

$$h_{VB}^+ + e_{CB}^- \rightarrow energy\ (heat) \qquad (2)$$

$$H_2O + h_{VB}^+ \rightarrow {}^*OH\ (hydroxyl\ radical) + H^+ \qquad (3)$$

$$O_2 + e^- \rightarrow O\ {}^*-\ (superoxide\ radical) \qquad (4)$$

$${}^*OH + Dye \rightarrow Intermediates \rightarrow H_2O + CO_2 \qquad (5)$$

$$O_2{}^*- + Dye \rightarrow Intermediates \rightarrow H_2O + CO_2 \qquad (6)$$
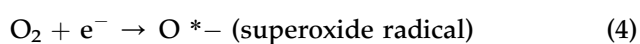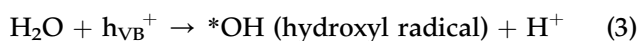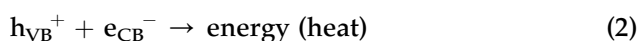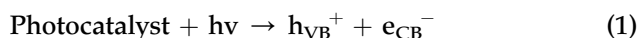
Metal oxide nanoparticles (including ZnO NPs) were created utilizing a variety of physical and chemical techniques such as milling, the sol–gel method, chemical vapor deposition, and many more [30,31]. Nevertheless, the implementation of

physio-chemical methods presents additional challenges, including concerns regarding toxicity, adverse environmental impacts, and the considerable costs associated with the necessary equipment [32,33]. To address these limitations, a viable alternative lies in the adoption of a biological approach utilizing organisms such as algae, fungi, bacteria, or plants, which offers the potential for producing non-toxic and cost-effective nanoparticles applicable in diverse fields like food, cosmetics, medicine, and wastewater treatment [34,35]. Plant extracts are rich in protein and phytochemical materials like sitosterol, luteolin, glycosides, flavonoids, and dexamethasone, which are considered reducing agents and stabilizers that have been successfully applied in research to produce ZnO NPs [36]. A variety of plants, including *Caccinia macranthera* [19], Passiflora caeruleafresh [37], peels of *Passiflora foetida* [38], *Portulaca oleracea* [39], *Tridax procumbens* Linn [40], *Tephrosia purpurea* [36], and Hibiscus rose [17] have used aqueous extracts of the (*T. purpurea*) *plant* to prepare ZnO NPs and examine the photocatalytic activity of these semiconductor nanoparticles to degrade methylene blue under sunlight.

The utilization of the green method, particularly eucalyptus leaves, for the synthesis of Zinc oxide nanoparticles (ZnO NPs) has been explored in limited studies. In this research, eucalyptus leaf extract was employed as a green reducing and capping agent to produce ZnO NPs. The efficiency of ZnO NPs in removing acid black 210 dye (AB210) from simulated wastewater was evaluated through adsorption and photocatalytic processes. The primary objective of this study is to investigate the degradation of acid black 210 (AB210) dyes in aqueous solutions using two approaches, namely adsorption and photocatalytic processes, with the utilization of a cost-effective and environmentally friendly catalyst.

1. The green synthesis of zinc oxide (ZnO-NPs) nanoparticles is environmentally friendly and prepared for the first time from eucalyptus leaves easily and economically. Eucalyptus trees are available locally and abundantly.
2. Design of a photoreactor using 24 UV-A lamps. It has a wavelength of 365 nm. It is located within the ultraviolet region (UV-A) of electromagnetic radiation, as most of the sun's rays that reach the earth are within the ultraviolet region (UV-A), and in the future, it is possible to rely on sunlight only as a source of energy as an alternative to using the photoreactor to investigate the degradation of the same dye (AB210) by the batch photocatalytic process.

2. Experimental

2.1. Chemicals

In this study, each of the chemical compounds used was of high purity (99.9%). The eucalyptus leaves used were picked up from the garden of Baghdad University, Iraq. The dye acid black 210 (AB210) was taken from the leather tanning factory (Karadaa Region). $ZnSO_4$ was obtained from a central drug house (CDH) in India, while 100% ethanol was obtained from (CARLO ERBA) reagents company in France.

2.2. Preparation of the leaf extract

The synthesis procedure was taken from Ref. [15] with slight modifications. Initially, the eucalyptus leaves were picked up and repeatedly washed for dust and difficult dirt removal using distilled water. The leaves were then dried for 12 h at 50 °C in the oven. The leaves were ground into a fine powder when they had thoroughly dried and become crushable. 150 mL of deionized water was used in the preparation of the extract using 10 g of eucalyptus leaves powdered. The eucalyptus leaves and deionized water were heated for 30 min at 80 °C. The resultant extract was cooled and filtered via filter paper; the filtrate was then kept at 4 °C until it was used in zinc oxide nanoparticles preparation.

2.3. Photocatalyst preparation

To prepare the ZnO NPs, 1.61 g of solid $ZnSO_4$ was mixed with 100 mL of deionized water and stirred vigorously at 150 rpm for 10 min. To remove contaminants, the solution was filtered using a 0.45 μm syringe filter. The eucalyptus extract was added gradually to the $ZnSO_4$ solution while continuously agitating it for 15 min at 70 °C. After the complete addition of the eucalyptus extract, the mixture was further agitated at 70 °C for 3 h, and the pH of the solution was adjusted to 12. The pH adjustment was achieved using a 1 M concentration solution of sulfuric acid and sodium hydroxide. The color of the mixture changes from dark yellow to light yellow. Demonstrates that ZnO NPs were created and that the reduction process took place. Vacuum filtration and numerous washes with distilled water and absolute ethanol were used to clear the yellow ZnO NPs precipitate. The yellow precipitate was dried at 80 °C and then ground into a fine powder using a mill and pestle.

2.4. Characterization of ZnO NPs

The characterization of ZnO NPs was analyzed using a variety of characterization techniques to determine their structure, shape, size, specific surface area, and other key characteristics. SEM was utilized to evaluate the size and form of the ZnO NPs (model Tescan Vega3, USA). The latter is used throughout conjunction with an energy-dispersive X-ray spectroscopy (EDX) examination that provides more details regarding the chemical components. Additionally, specific surface area, pore size, and pore volume were determined using the Brunauer, Emmett, Teller (BET) analysis (TriStar II Plus version 2.03 instrument, USA). Finally, the Fourier transform infrared (FT-IR) spectroscopy was applied to examine the functional groups of ZnO NPs (Shimadzu, Japan).

2.5. Design of photoreactor

The photoreactor is designed to accomplish the photocatalysis process under UV- light radiation type A. 24 UV-A lamps (30 cm long, 2.2 cm broad, 8 W of power, 1 W/m^2 of light intensity, and a maximum wavelength peak of 365 nm) were put within a cylindrical aluminum container to create a reflecting surface for incident photons. The aluminum container is attached to a cube of wood with dimensions of (60 × 60 × 60 cm), and the spacing between the lights and the reaction room was reduced to ten centimeters. The photoreactor has two fans installed at the top that supplies cooling air and protects the reaction vessel from the hot lamps; the temperature within the reactor is regulated between 30 and 40 °C.

The temperature inside the reaction cell and the light reactor was tracked using nine thermocouples evenly distributed throughout the device. The layout of the photoreactor is shown in Fig. 1.

2.6. Fixed bed design

Batch experiments of AB210 removal through an adsorption and photocatalytic process were carried out in a beaker Pyrex of 1 L. The effect of several operational parameters was studied during both processes, including pH ranging (2–9), the temperature ranging (25–55 °C), AB210 concentration ranging from (5–40 mg/L) and the amount of ZnO NPs within the range of (0.1–1 g/L). Initially, 1 M sulfuric acid and 1 M sodium hydroxide were utilized to make adjustments the pH of solutions. Accordingly, in the adsorption process, ZnO NPs
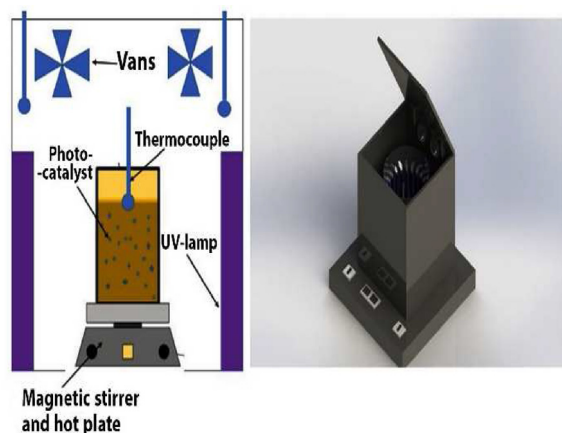
Fig. 1. Schematic diagram of photoreactor.

Fig. 2. FT-IR of ZnO NPs.

were added to the dye solution and magnetic agitated for 2 min and at a temperature of 25 °C to enable the ZnO NPs to be diffused homogeneously inside the solution. The photocatalytic process was performed using a photo reactor, shown in Fig. 1. The samples were obtained at regular intervals during the experiment and purified using a 0.45 μm syringe filter. Finally, A UV/Vis spectrophotometer was used to measure the concentration of AB210 at a wavelength of 465 nm. The following equation was used to determine the removal effectiveness of AB210.

$$\%DR = \frac{C_o - C_t}{C_o} x\ 100\ \% \tag{7}$$

where $\%\ DR$ is the removal efficiency, C_o is initial AB210 (mg/L) and final C_t is AB210 at time.

3. Results and discussion

3.1. Characterization of ZnO NPs

ZnO NPs functional groups were defined by (FT-IR) using a mid-IR spectrum (400-4000 cm^{-1}), as depicted in Fig. 2. Significant eucalyptus leaves extract peaks to exhibit a broad band at 3414 and 3425.5 cm^{-1} because of the O−H stretching of polyphenols [41,42].

The following band at 1543 cm^{-1} is associated with aromatic C=C stretching [43,44]. Also, the band at 1481.3 cm^{-1} is caused by the presence of the tertiary alcohol (C−OH) group. A thin, narrow absorption band shows C−O stretching vibrations of carboxylic acids at 1045.4 cm^{-1} (COOH). Similarly, peaks have been observed at 869.9 cm^{-1} corresponding to the isoprenoids and organic acid in eucalyptus extract [27,45]. These functional groups explain the presence of biomolecules in eucalyptus
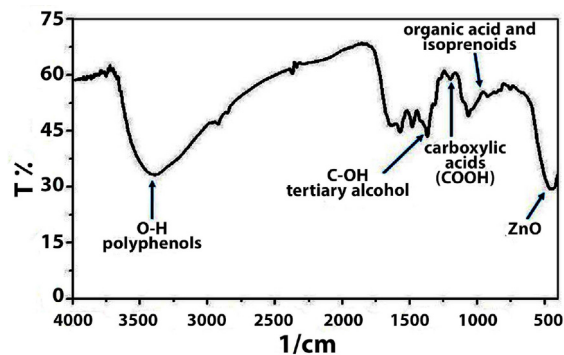
extract that serve as a capping agent to prevent the aggregation of NPs. There are peaks between 439.7 and 416.6 cm^{-1} that indicate ZnO NPs [46,47].

The band gap energy of ZnO NPs was examined using a UV−Visible spectroscopy method analysis at wavelengths ranging from 200 to 700 nm, with the maximum peak at 358 nm and the band gap energy was calculated using the equation $E_g = \frac{hc}{\lambda}$, where h Planck's constant $= 6.626 \times 10^{-34}$ J s, C is the velocity
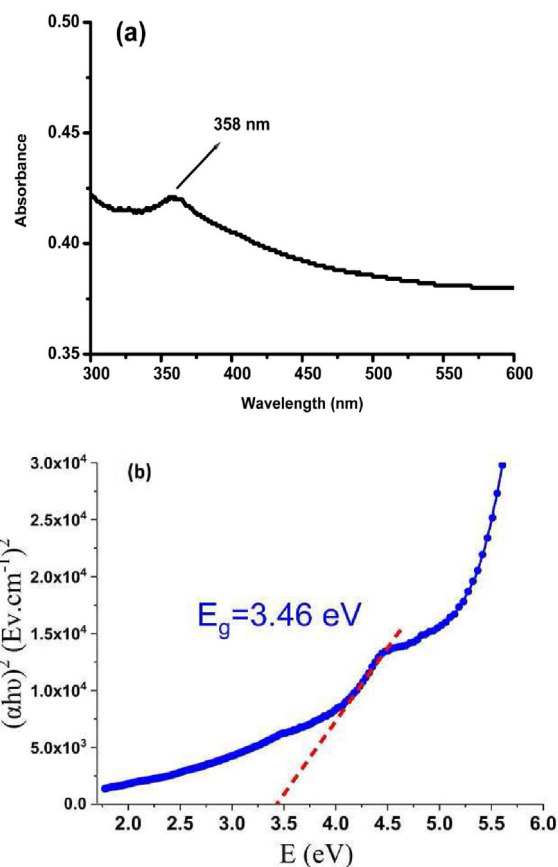

Fig. 3. (a) UV−Visible absorption spectra (b) band gap energy diagram of ZnO NPs.

of light $= 3 \times 10^8$ m/s and λ corresponds to the wavelength of the peak with maximum intensity, The maximum wavelength is 3.46 eV, which is consistent with recent results [48,49] (see Fig. 3).

The fundamental process of photocatalyst activation is shown in Fig. 4.

In order to do this, photons with energies ($=$hv) greater than a photocatalyst's band gap (BG) must be absorbed. This causes electrons (e^-) to move from the valence band to the conduction band, creating a hole (h^+) in the valence band. These divided holes and electrons can, However, these separated holes and electrons can recombine and release the absorbed energy as heat. These photogenerated e^- and h^+ then react with easily accessible oxidants and reductants to form powerful and unstable radicals, which react with the contaminant and mineralize it to carbon dioxide and water while also producing a variety of intermediary species [29].

The scanning electron microscopy (SEM) analysis of ZnO nanoparticles (NPs) revealed their predominantly porous and spherical morphology, exhibiting a range of sizes spanning from 22 to 37 nm, as visually depicted in Fig. 5. Moreover, the presence of polyphenol as a capping agent played a pivotal role in encapsulating the surface of ZnO NPs. This protective coating contributed to minimal agglomeration, thereby observed through SEM analysis [48,50]. Additionally, the (EDAX) analysis illustrated the constituents and chemical composition of ZnO NPs.

According to Fig. 6, Zinc, oxygen, and gold are present in the sample, according to the ZnO NPs EDAX analysis. The elevated intensities of the zinc and oxygen peaks indicate that ZnO constitutes the bulk of the sample. In the ZnO NPs sample, the weight percentages of zinc, oxygen, and gold were 73.4%, 4.619%, and 21.97%, respectively. Zinc's atomic percent was 59.32%, and oxygen's atomic percent was 29.26%. However, O indicated that polyphenols and other organic compounds were present in the eucalyptus leaf extract [51]. The application of a sample coating for SEM imaging resulted in the presence of gold. Furthermore, the analysis of the EDAX spectrum revealed the existence of two distinct peaks corresponding to zinc at energy levels of one keV and 8.7 keV, alongside a solitary peak representing oxygen at a wavelength of 0.5 keV. These observations suggest the presence of zinc in the form of zinc oxide nanoparticles (ZnO NPs) [16,52].

ZnO NPs' specific surface area (SSA), pore size, and pore volume were assessed using (BET). Pore volume, SSA, and dimension were 26.318 m^2/g, 0.098 cm^3/g, and 11.118 nm, respectively. The findings demonstrate that ZnO NPs are mesoporous particles because the pore size is in the mesoporous particles [53,54]. The high SSA shows the potential for inexpensive ZnO NPs to absorb contaminants [55].

Zeta potential determination is a critical indicator for assessing particle stability. A high zeta potential indicates that nanoparticles are stable and resistant to aggregation. Conversely, a low zeta potential suggests that nanoparticles are unstable and prone to flocculation. Fig. 7 demonstrates the zeta potential analysis, which yielded a significantly negative value of -72.28 mV, indicating the excellent stability of ZnO NPs [56]. This stability can be attributed to the presence of phenolic chemicals in the eucalyptus leaf extract [57].

Fig. 8 illustrates 20 the characteristic peaks of ZnO NPs. at 31.59°, 34.56°, 36.35°, 47.65°, 56.65°, 62.85° and 68.45°, for (010), (002), (011), (012), (110), (013), (021) planes of the crystal lattice, respectively [58], By comparing the results from Joint Committee on Powder Diffraction Standards (JCPDS) card No. 89−7102, The spherical and hexagonal zinc oxide phases are responsible for all the diffraction peaks. The product possesses a well-crystalline particle structure, as seen by the diffraction peaks that are both narrow and robust [58].
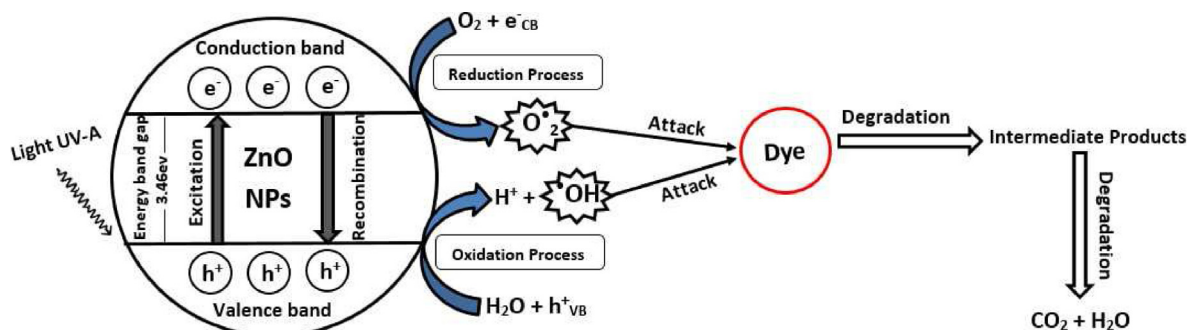

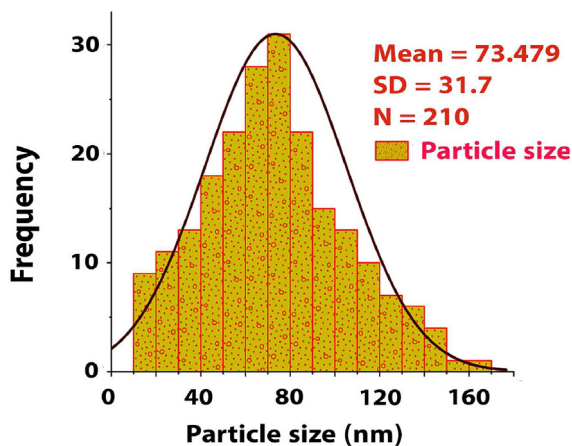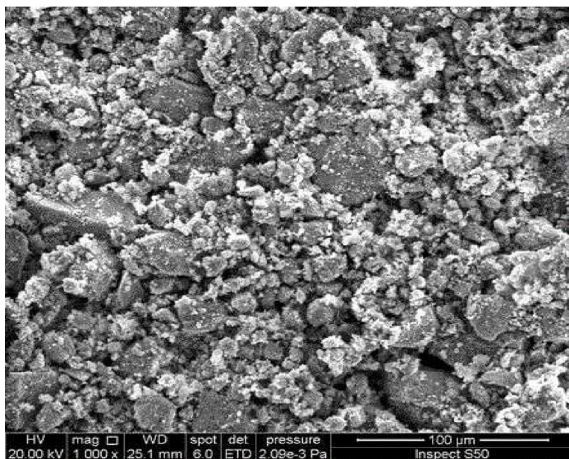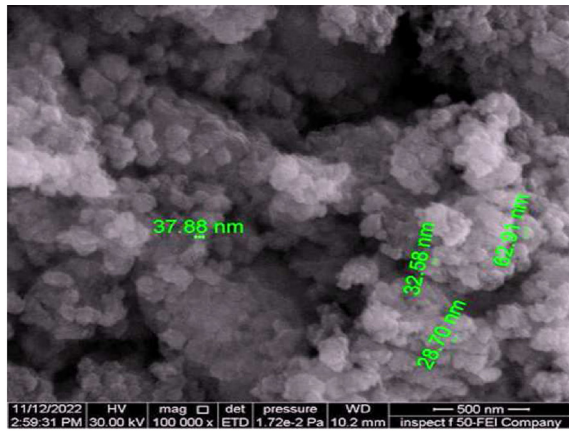*Fig. 4. Basic principle of photocatalysis.*

Fig. 5. SEM image of ZnO NPs.

3.2. Effect of parameters on adsorption and photo catalytic process

3.2.1. Effect of the ZnO-NPs

Fig. 9a illustrates the removal efficiency of AB210 13,16,18,20, and 22% after 300 min of adsorption experiments for doses of 0.1, 0.25, 0.5, 0.7, and 1.0 g/L, respectively. The effect of the catalyst dose on the
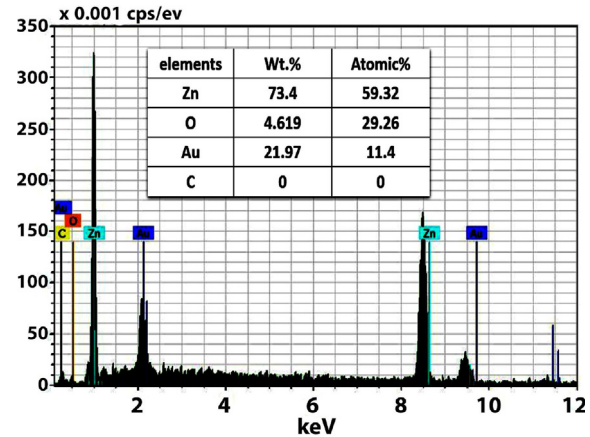

Fig. 6. EDAX results of ZnO NPs.

breakdown of AB210 was investigated. The nanoparticle dose was changed between (0.1−1 g/L) while maintaining the other operational conditions' parameters constant. From the other side, a greater surface area and active site on the ZnO NPs surface resulted in increased removal effectiveness and efficiency at higher ZnO NPs doses [59,60] After reaching equilibrium, expanding these sites had no further effect so, the removal rate increased slowly.

On the other hand, the photo-degradation process exhibited different outcomes, as illustrated in Fig. 9b. The removal efficiencies observed for the corresponding doses in the adsorption experiments were 33%, 47%, 64%, 66%, and 68%, respectively. These findings indicate that the initial rate of photo-degradation escalated in proportion to the catalyst loading. This phenomenon can be attributed to the higher catalyst dosage, which effectively augmented the total surface area, subsequently leading to an increased number of active sites. Furthermore, the quantity of hydroxyl and superoxide radicals
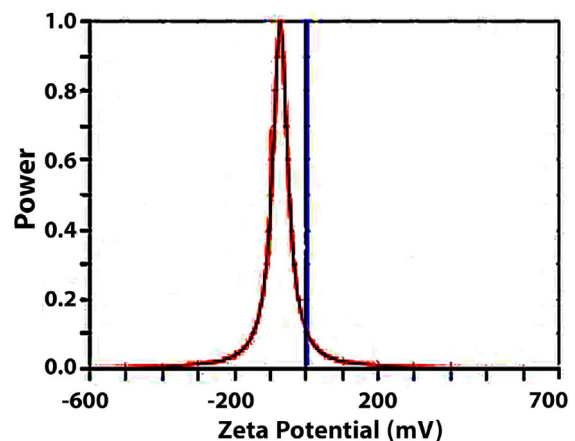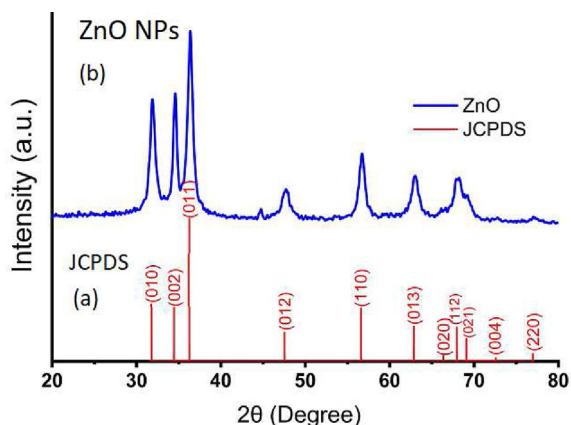

Fig. 7. Zeta potential of ZnO NPs.

Fig. 8. XRD patterns of synthesized ZnO nanoparticles: (a) Standard XRD pattern and (b) ZnO NPs XRD pattern.

increased, which contributes to removal of organic contaminants [53,61]. Economically side, 0.75 g/L of ZnO NPs was determined to be the ideal quantity for both processes due to the closest removal efficiency at 1 g/L of ZnO NPs.

3.2.2. Effect of pH

The charge on the catalyst surface highly depends on the acidity, neutrality, or basicity of the dye solution, and this has a massive effect on dye removal. As Fig. 10a shows, the removal rate of AB210 was studied at the pH range (2–9) by keeping other operating conditions constant. The AB210 removal efficiencies were 13, 16, 21, 34, 31, and 26% for pH 2, 3, 4, 5, 7, and 9, respectively.

At low pH (2 and 3), ZnO NPs partly dissolve, reducing the active sites on the catalyst surface and ZnO NPs' removal efficiency. Additionally, at a basic pH of 9, the hydroxyl ion and AB210 molecules compete for the active sites on ZnO NPs, which lowers the removal efficiency [62].

Moreover, Fig. 10b shows, the photo-degradation process, the AB210 removal rates increased from 38 to 74% when pH increased from 2 to 7 and decreased to 73% at pH 9. This phenomenon is due to the fact that AB210 is an anionic dye, and the repulsion between the catalyst's molecules and dye molecules will develop at an acidic pH where the ZnO NPs surface and dye molecules are both
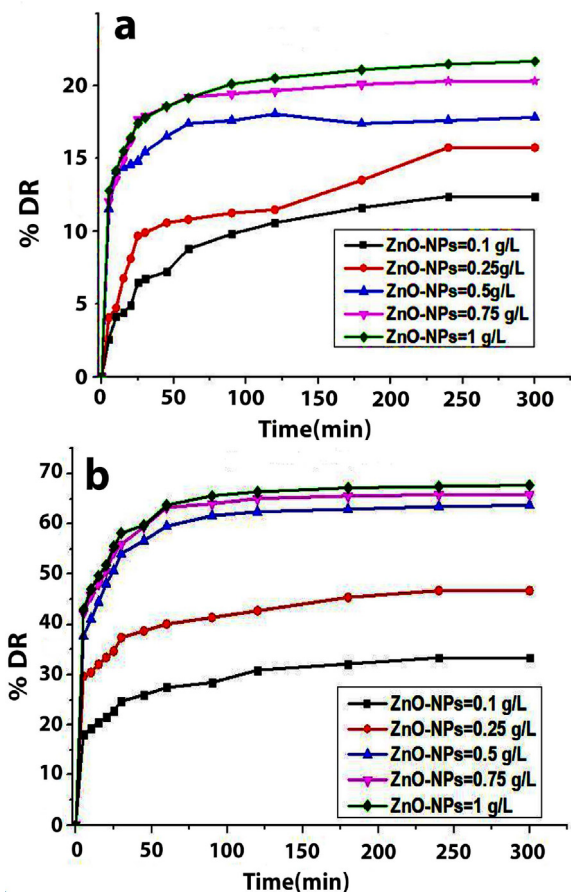

Fig. 9. The effect of ZnO NPs amount at initial AB210 concentration, pH, and temperature of 25 mg/L, 4,5 and 25 °C respectively, (a) adsorption process, (b) photocatalytic process.
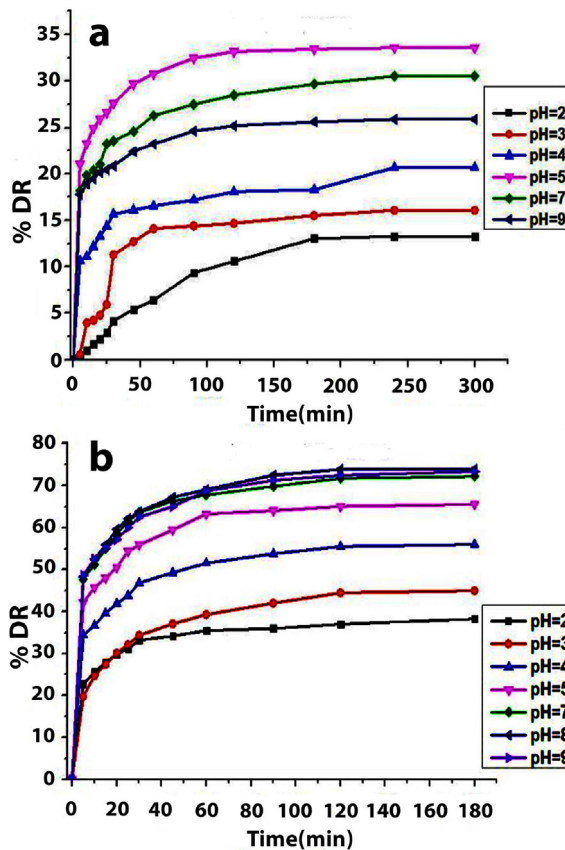

Fig. 10. The effect of initial pH at ZnO NPs dose, temperature and initial AB210 concentration were 0.75 g/L, 25 mg/L, and 25 °C, (a) adsorption process, (b) photocatalytic process.

positively charged. Whereas the repulsion between the AB210 and ZnO NPs decreased with increasing pH to a specific extent [63,64]. Decreasing the degradation at alkaline (pH 9) is due to the negative charge of ZnO NPs at this pH, leading to an increase in the repulsion effect [33,65]. As a result, 5 and 7 were selected as the ideal pH for the adsorption and photocatalysis processes, respectively.

3.2.3. Effect of temperature

The temperature of the experiments was changed to a range of (35–55 °C) by retaining all other operation parameters constant. As seen in Fig. 11a, the removal efficiencies of AB210 during the adsorption procedure ranged from 33.5% to 55.1% when the temperature increased from 25 to 55 °C. At increasing temperatures, more active sites become available, and the adsorbent surface becomes activated explaining the increase in the removal of AB210. In addition, the dye molecules obtained the necessary energy at higher temperatures because of the enhanced diffusion and mobility of AB210 dye ions from the bulk solution to the surface of ZnO NPs [66]. Fig. 11b indicates that during the photo degradation process, the removal rate of AB210 was 72.1, 75.7, 78.1 and 80.76% at a temperature of 25, 35, 45, and 55 °C. Actually, increasing temperature leads to faster photocatalytic reaction and hence increase the production of •OH [67].

3.2.4. Effect of UV intensity

Fig. 12 shows that for UV intensities of 6, 15, and 24 W/m^2, respectively, the removal rates of AB210 were 70, 78, and 86%. The removing efficacy enhanced as the UV intensity increased because it generated more photons, causing more electron–hole pairs to be excited [47]. The UV intensity of 24 W/m^2 so was selected as the best UV intensity.

3.2.5. Effect of initial AB210 concentration

Initial dye concentration is an important parameter to research because it takes into account a force that will accelerate the transition between the solid and liquid phases. As a result, the effects of AB210 concentrations removal efficiency were studied at a range of (5–40 mg/L), while keeping the other operation conditions at optimum values. At AB210 from concentrations of (5–40) mg/L, the removal rates were, correspondingly, 62, 60, 50, 40, and 37%, as shown in Fig. 13a. The outcomes demonstrated maximal removal at 5 and 10 mg/L due to the availability of vacant sites. Rising AB210 concentration of more than 10 mg/L cause more dyes molecules to go toward these open nanoparticle locations then the amount of accessible active sites in the adsorbent decreases,

resulting in a reduced AB210 removal efficiency [12,68].

On the other side, the photocatalytic degradation in the same range of dye concentration gave removal efficiency of 100, 98, 91, 87, 84.5 and 80% at AB210 concentrations of (5–40) mg/L, respectively, as shown in Fig. 13b. Basically, (Beer–Lambert's) law states that light absorption rises with dye concentration, preventing more photons, particularly in the deeper part of the solution, from reaching the catalyst surface. Therefore, it is expected that both the production of charge carriers and the degradation efficiency would diminish, resulting in a decline in •OH production and subsequently reducing the overall removal efficiency [69]. Furthermore, the photocatalytic process heavily relies on the presence of active sites, and an increase in the initial concentration of AB210 would result in a decrease in the availability of accessible active sites [18].

3.3. Adsorption kinetics

In the kinetic investigation, pseudo-first order, pseudo-second order, and Elovich models were
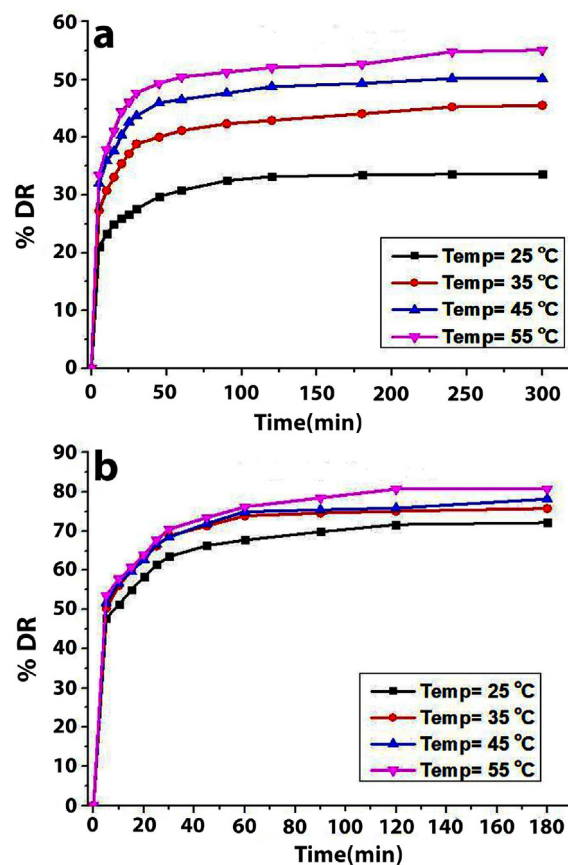

Fig. 11. The effect of temperature at ZnO NPs dose, initial concentration AB210, pH were 0.75 g/L, 25 mg/L, and 5,7 respectively, (a) adsorption process (b) photocatalytic process.
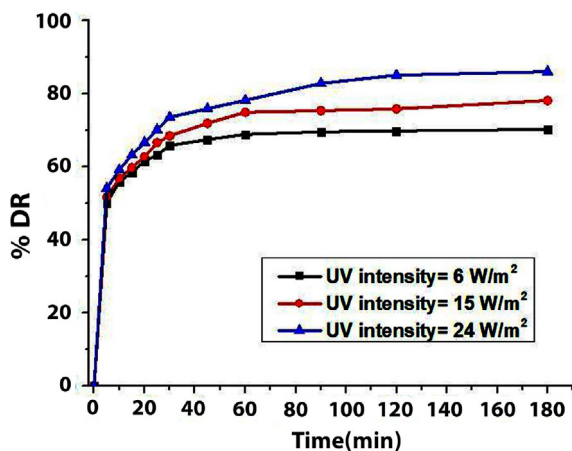
Fig. 12. Effect of UV-intensity on photocatalytic process at ZnO NPs dose, initial concentration AB210, pH, and temperature were 0.75 g/L, 25 mg/L, 5, 7 and 45 °C respectively.

utilized to calculate the adsorption data. Equations 8–10 present the kinetic equations employed to analyze the adsorption kinetics [70]. Plotting log (q_e-q_t) versus time (t) yields the constant rate k1
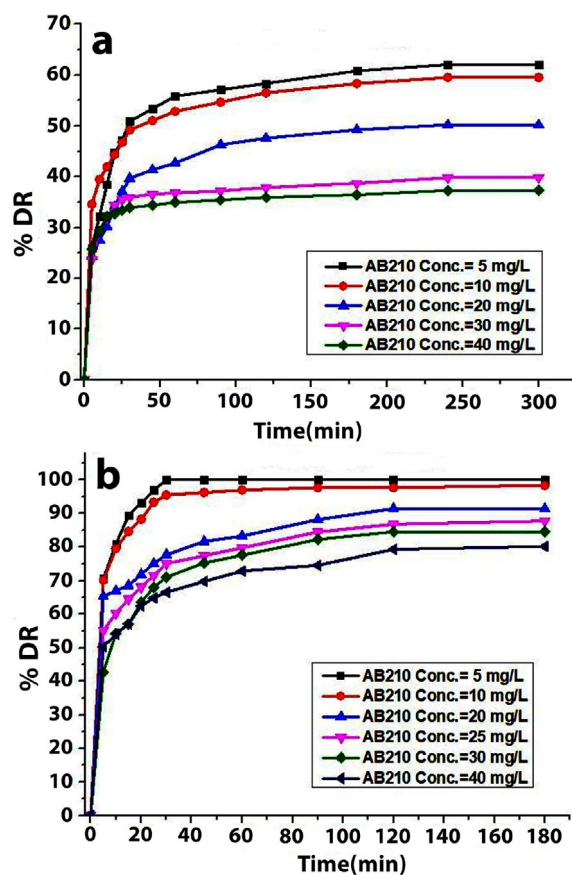

Fig. 13. Effect of initial concentration AB210 at ZnO NPs dose, pH, and temperature were 0.75 g/L, 5 and 7, 15 W/m² and 45 °C respectively, (a) adsorption process (b) photocatalytic process.

pseudo-first order model, as shown in Fig. 14a. Additionally, by plotting t/versus t, it was possible to calculate the slope k_2 and intercept q_e of pseudo-second order (see Fig. 14b). Additionally, systems with heterogeneous adsorbing surfaces can benefit from the Elovich model in chemical adsorption research [71]. As shown in Fig. 14c, where and are the adsorption and desorption rate factors, the intercept and slope between and ln (t) allowed for the determination of and in the Elovich equation.t Table 1 shows, that the of α and β are affected by changing the AB210 concentration. As a result, when the AB210 concentration raised from 5 to 40 mg/L, the β decreased, and without notable variation in α. Furthermore, the results demonstrated that the adsorption rate is greater than the desorption constant β, indicating the viability of adsorption. Moreover, the Elovich model's R^2 was already low, indicating the model's poor fit. R^2 for pseudo-second order is greater than R^2 for pseudo-first order, indicating that the pseudo-second order kinetic model is fitted to the adsorption process by ZnO NPs. According to Table 1, Pseudo-second-order is perfectly suited to explain the kinetics of the ZnO NPs system.

$$\text{Pseudo}-\text{first order}\quad \log\left(q_e - q_t\right) = \log q_e - \frac{k_{1\,t}}{2.303} \quad (8)$$

$$\text{Pseudo}-\text{second order}\quad \frac{t}{q_t} = \frac{1}{k_2\,q_e^2} + \frac{t}{q_e} \quad (9)$$

$$\text{Elovich}\quad\quad q_t = \frac{1}{\beta}In(\alpha\beta) + \frac{1}{\beta}In(t) \quad (10)$$

Where, q_t: adsorption capacities at time t (mg. g^{-1}), k_1: pseudo-first-order rate constant (min^{-1}), k_2: pseudo-second-order rate constant (min^{-1}), and α: initial adsorption rate (mg. [g. min]$^{-1}$).

3.4. Adsorption thermodynamic

The AB210 adsorption onto ZnO NPs was studied at different temperatures (20, 35, 45, 55 °C) to establish the spontaneity, nature, and application of the adsorption. These adsorption qualities can be determined using standard Gibbs free energy (Δ $G°$), standard enthalpy (Δ $H°$), and standard entropy (Δ $S°$) thermodynamic factors, which were obtained from the equations below [72,73].

$$\Delta G^o = \Delta H^o - T\Delta S^o \quad\quad\quad (11)$$

$$\Delta G^o = -RTlnK_c \quad\quad\quad (12)$$
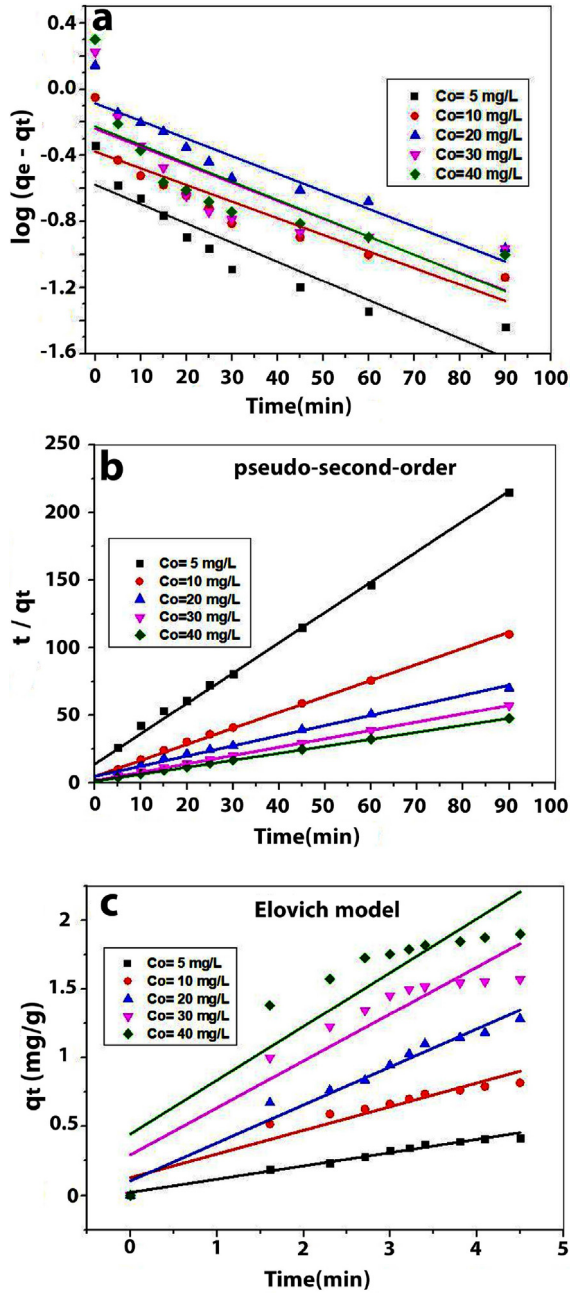
Fig. 14. Kinetics models (a) pseudo-first-order, (b) pseudo-second-order, and (c) Elovich model.

$$K_c = \frac{q_e}{C_e} \tag{13}$$

K_C is known as the distribution constant (L/g). Similarly, as shown in Fig. 15a, $\Delta S°$ and $\Delta H°$ can be computed using the intercept and slope of the graph of $\Delta G°$ vs temperature (K). In addition, the Arrhenius equation described below can also be used to calculate the actvation energy.

$$lnk_{obs} = lnA - \frac{E_a}{RT} \tag{14}$$

$$\ln\left(\frac{C_t}{C_o}\right) = -k_{obs}t \tag{15}$$

Where E_a is activation energy (kJ/mol), A is Arrhenius constant ($J.mol^{-1}k^{-1}$), and k_{obs} are the rate constant (min^{-1}).Fig. 15b illustrates the plot slope between ln (k_{obs}) and $1/T$ as represented by activation energy Ea. Table 2 illustrate the thermodynamic characteristics of the AB210 adsorption onto ZnO NPs. At the investigated optimum temperature, the Gibbs free energy ($\Delta G°$) was −0.782 kJ/mol, which had a negative value demonstrating spontaneous of the adsorption process [74].

The adsorption of AB210 onto ZnO NPs was revealed to be an endothermic process at the solid−solution interface, and the AB210 ions had a
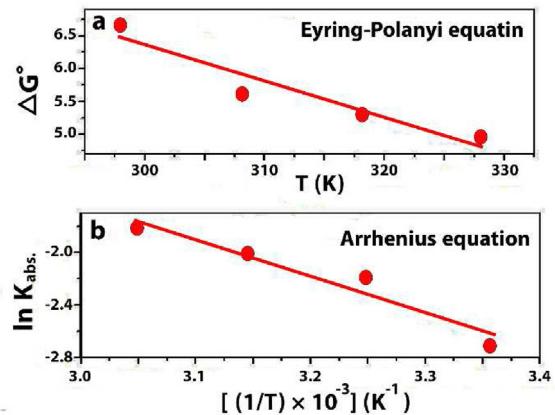
Fig. 15. Linear form of (a) Eyring Polanyi equation, (b) Arrhenius equation.

Table 1. Parameters of adsorption kinetics of AB210 onto ZnO NPs.

AB 210 mg/L	Pseudo-first order		Pseudo-second order		Elovich		
	k_1	R^2	k_2	R^2	α	β	R^2
5	0.026	0.86	0.37	0.992	0.12	10.36	0.98
10	0.023	0.81	0.319	0.996	0.364	5.814	0.91
20	0.024	0.9	0.125	0.99	0.405	3.62	0.97
30	0.025	0.64	0.299	0.999	0.809	2.927	0.87
40	0.026	0.65	0.32	0.999	1.224	2.553	0.81

Table 2. Thermodynamic factors.

Factors	Values
$\Delta G°$ (kJ/mol) at 45 °C	−0.782
$\Delta H°$ (KJ/mol)	26.93
$\Delta S°$ (kJ/mol.K)	0.086
Ea (KJ/mol)	26.913
A (J/mol.K)	3.439×10^3

suitable affinity for nanoparticles thanks to a positive value for H° (26.93 kJ.mol-1). The result of (S°) was favorable (0.086 kJ. mol.), indicating an appropriate affinity of AB210 ions for nanoparticles and spontaneous interference in the process of adsorption at the solid–liquid interface.

4. Conclusion

In conclusion, this study effectively demonstrated the efficacy of employing Eucalyptus plant extract for the environmentally friendly synthesis of Zinc oxide nanoparticles (ZnO NPs). A comprehensive array of analytical techniques, encompassing UV–Vis spectroscopy, FT-IR analysis, XRD, SEM, EDAX, BET, and Zeta potential, was utilized to assess the properties and quality of the biofabricated ZnO NPs. The characterization findings unveiled a porous nanoparticle architecture of the ZnO NPs, with an average dimension of 73.4 nm and a specific surface area of 26.318 m^2/g. XRD analysis verified the crystalline structure of the nanoparticles, while FT-IR results confirmed the presence of distinct polyphenolic groups.

The synthesized Zinc oxide nanoparticles (ZnO NPs) were utilized for the degradation of AB210 dye through adsorption and photocatalytic reactions. The photocatalytic process exhibited remarkable efficiency in comparison to adsorption, achieving a complete removal efficiency of 100%. In contrast, the adsorption process demonstrated a removal efficiency of 62%. Thermodynamic and kinetic investigations revealed that the adsorption process involved physisorption, characterized by an endothermic nature, and the pseudo-second-order model kinetics accurately represented the experimental data.

The green synthesis approach highlighted in this research holds promise for enhancing the photocatalytic activity of ZnO NPs, particularly for the removal of diverse organic pollutants from wastewater. This study presents a cost-effective and environmentally responsible method for water purification. Moreover, the catalyst's catalytic capacity and the established quadratic patterns for batch and continuous systems could serve as valuable foundations for future investigations in this field.

Conflicts of interest

The authors declare no Conflict of interest.

Acknowledgements

Appendix A. Supplementary Materials

S1. Adsorption isotherm

The maximum adsorption rate of adsorbates and adsorbents is frequently calculated using the adsorption isotherm. formulas (17-20) are used to analyze the interaction between ZnO NPs (the adsorbent) and AB210 (the adsorbed dye) in the Langmuir, Temkin, Freundlich, and Dubinin isotherm model, Table A (in appendix) lists the adsorption isotherm parameters. The slope and intercept can be determined by plot 1/q_e vs 1/C_e to get the Langmuir parameters of q_{max} and K_L. Additionally, the separation factor R_L is a dimensionless constant that serves as a good predictor of the Langmuir isotherm; the equation that yields this expression is as follows:

$$R_L = \frac{1}{1 + K_L C_o} \tag{16}$$

If R_L is greater than one, the adsorption is favorable, whereas the adsorption is considered unfavorable if R_L is smaller than one. On the other hand, $R_L = 0$ irreversible adsorption and $R_L = 1$ for linear one [75,76].

Additionally, the slope and intercept can be determined by the plot of the graph of Log Ce vs Log K_F can be used to determine 1/n and K_F parameters of the Freundlich isotherm. Additionally, the values of 1/n can be utilized to understand the nature of adsorption. When 1/n = 0, the adsorption is irreversible or considered favorable when 0 > 1/n > 1 and unfavorable when 1/n < 1. Fig. 14 displays the isotherm models. The isotherm data in Table S1 showed that the R_L values are ranging (0 > R_L 1>) and that the Langmuir model has a high regression coefficient (R^2 = 0.9964). These two variables demonstrated a favorable isotherm as well as a high level of interaction between the AB210 and the catalyst. Additionally, the value of 1/n between 0 and 1 indicates a favorable isotherm, and Freundlich constant K_F, which has a substantial value (0.6217), is another indication from the Freundlich isotherm and predicts increased adsorption capability. According to the Temkin isotherm, the highest binding heat of sorption B_T was positive (0.5978 kJ mol^{-1}), which denotes an exothermic adsorption process, Temkin model doesn't fit the data since this isotherm has a component that

specifically accounts for adsorbent–adsorbate interactions, by neglecting the extremely low and high concentration values [77,78]. Good R^2 obtained from the Dubinin isotherm is also higher ($R^2 = 0.91$), indicating a significant interaction between the reactive group of AB210 and the ZnO NPs. Additionally, E value was (0.631 kJ/mol), which further demonstrated that the adsorption type is physisorption [79].

$$\text{Langmuir} \quad \frac{1}{q_e} = \frac{1}{q_{max}.K_L}\left(\frac{1}{C_e}\right) + \frac{1}{q_{max}} \quad (17)$$

$$\text{Freundlich} \quad \log q_e = \left(\frac{1}{n}\right)\log C_e + \log K_F \quad (18)$$

$$\text{Temkin} \quad q_e = B_T \ln C_e + B_T \ln K_T, \quad (19)$$

$$\text{Dubinin} \quad nq_e = \ln q_m - \beta \varepsilon^2 \quad (20)$$

where,

q_{max}: Saturation adsorption of Langmuir (mg.L^{-1}).

K_L: Equilibrium constant of Langmuir (L.mg^{-1}).

K_F: The Freundlich adsorption constants.

$1/n$: Factor of heterogeneity, K_T: Factor of maximum binding energy (L.g^{-1}).

B_T: Maximum binding heat of sorption (KJ.mol^{-1}).

$B_T = \frac{RT}{b_T}$.

R: Ideal gas constant ($0.008314 \text{ Kj. mol}^{-1}. \text{K}^{-1}$).

T: Absolute temperature (K).

q_m: The theoretical saturation capacity.

β: Dubinin constant ($\text{mol}^2. \text{Kj}^{-2}$).

ε: Dubinin isotherm constant $\epsilon = RT \ln\left(1 + \frac{1}{C_e}\right)$.,

E: Adsorption energy (kJ.mol^{-1}), $E = \frac{1}{\sqrt{(2\beta)}}$.

Table S1. Parameters of adsorption isotherm of AB210 onto ZnO-NPs at different concentration (AB210).

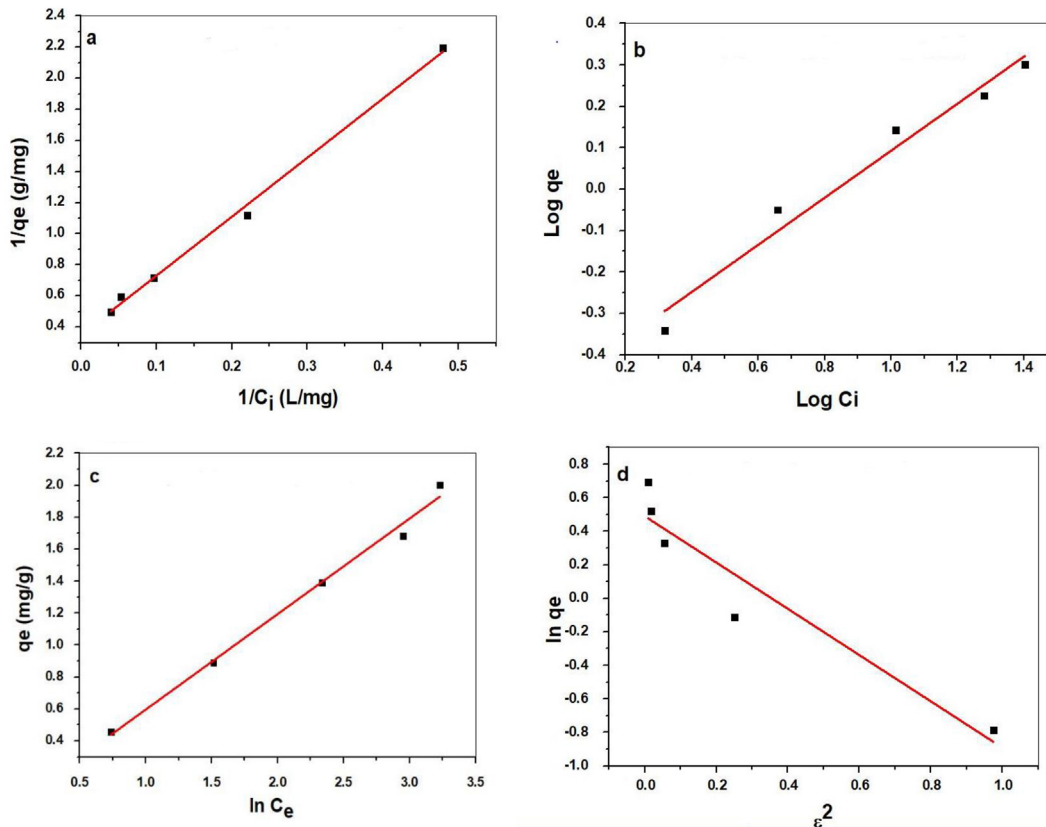| Langmuir			Freundlich				Temkin			Dubinin			
q_{max}	K_L	R^2	R_L	K_F	$\frac{1}{n}$	R^2	K_T	B_T	R^2	q_m	β	E	R^2
2.84	0.092	0.996	0.662	0.62	0.568	0.97	0.99	0.59	0.99	1.63	1.37	0.6	0.91

Fig. S1. Isotherm models (a) Langmuir model, (b) Freundlich model, (c) Temkin model, (d) Dubinin model.

References

[1] E.S. Önal, T. Yatkin, M. Ergüt, A. Özer, Green synthesis of iron nanoparticles by aqueous extract of eriobotrya japonica leaves as a heterogeneous Fenton-like catalyst: degradation of basic red 46, Int. J. Chem. Eng. Appl. 8 (2017) 327—333.

[2] P. Taylor, S.S. Sonawane, S. Mishra, N.G. Shimpi, Polymer-plastics technology and engineering effect of nano-$CaCO_3$ on mechanical and thermal properties of polyamide nano-composites effect of Nano- $CaCO_3$ on Mechanical and Thermal Properties of Polyamide, Nanocomposites 49 (2010) 37—41.

[3] N. Kataria, V.K. Garg, M. Jain, K. Kadirvelu, Preparation, characterization and potential use of flower shaped Zinc oxide nanoparticles (ZON) for the adsorption of Victoria Blue B dye from aqueous solution, Adv. Powder Technol. 27 (2016) 1180—1188.

[4] M. Jha, N.G. Shimpi, S.S. Sonawane, Journal of Genetic Engineering and Biotechnology Green synthesis of zero valent colloidal nanosilver targeting A549 lung cancer cell : in vitro cytotoxicity, J. Genet. Eng. Biotechnol. 16 (2018) 1—10.

[5] M. Batool, S. Khurshid, Z. Qureshi, W.M. Daoush, Adsorption, antimicrobial and wound healing activities of bio-synthesised zinc oxide nanoparticles, Chem. Pap. 75 (2021) 893—907.

[6] S. Jain, A.P. Shah, N.G. Shimpi, An efficient photocatalytic degradation of organic dyes under visible light using zinc stannate (Zn_2SnO_4) nanorods prepared by microwave irradiation, Nano-Struct. Nano-Obj. 21 (2020) 100410.

[7] Z.A. Mahmoud, M.A. Atyia, A.K. Hassan, The influence of support materials on the photo-Fenton-like degradation of azo dye using continuous nanoparticles fixed-bed Column, 2022, pp. 14—31, 18.

[8] O.H. Fadhel, M.Y. Eisa, Z.R. Zair, Decolorizing of malachite green dye by adsorption using corn leaves as adsorbent material, J. Eng. 27 (2021) 1—12.

[9] M. Jha, S. Ansari, N.G. Shimpi, Ultrasonic assisted green synthesis of Ag:CdO nanocubes and nanospheres using Citrus limon leaves for efficient degradation of organic dyes, J. Ind. Eng. Chem. 69 (2019) 269—284.

[10] Arsou Arimi, Lena Megatif, Luis I. Granone, Ralf Dillert, Detlef W. Bahnemann, Visible-light photocatalytic activity of zinc ferrites, J. Photochem. Photobiol. A 6030 (17) (2018) 31671—31674.

[11] P. Taylor, S.S. Sonawane, S. Mishra, N.G. Shimpi, A.P. Rathod, K.L. Wasewar, Polymer-plastics technology and engineering comparative study of the mechanical and thermal properties of polyamide-66 filled with commercial and nano-Mg $(OH)_2$ particles comparative study of the mechanical and thermal properties of polyamide-66 Filled with Commercial, 2014, pp. 37—41, 49.

[12] Z. Monsef Khoshhesab, S. Souhani, Adsorptive removal of reactive dyes from aqueous solutions using zinc oxide nanoparticles, J. Chinese Chem. Soc. 65 (2018) 1482—1490.

[13] M. Alkasir, N. Samadi, Z. Sabouri, Z. Mardani, M. Khatami, M. Darroudi, Evaluation cytotoxicity effects of biosynthesized zinc oxide nanoparticles using aqueous Linum Usitatissimum extract and investigation of their photocatalytic activityackn, Inorg. Chem. Commun. 119 (2020) 108066.

[14] T.H. Saleh, S.T. Hashim, S.N. Malik, B.A. Laftaah Al-Rubaii, Down-regulation of fliL gene expression by Ag nanoparticles and TiO_2 nanoparticles in pragmatic clinical isolates of Proteus mirabilis and Proteus vulgaris from urinary tract infection, Nano. Biomed. Eng. 11 (2019) 321—332.

[15] B.I. Dheeb, S.M.A. Al-Dujayli, I.M. Ibrahim, Q.A. Abbas, A.H. Ali, A. Ramizy, M.H. Eisa, A.I. Aljameel, I.M. Ali, B.M. Khashman, A.F. Hussain, Study the antifungal activity of ZnS:Mn nanoparticles against some isolated pathogenic fungi, J. Phys. Conf. Ser. 1178 (2019) 012008.

[16] A.A. Barzinjy, H.H. Azeez, Green synthesis and characterization of zinc oxide nanoparticles using Eucalyptus globulus Labill . leaf extract and zinc nitrate hexahydrate salt, SN Appl. Sci. 2 (2020) 1—14.

[17] Kainat, M.A. Khan, F. Ali, S. Faisal, M. Rizwan, Z. Hussain, N. Zaman, Z. Afsheen, M.N. Uddin, N. Bibi, Exploring the therapeutic potential of Hibiscus rosa sinensis synthesized cobalt oxide (Co_3O_4-NPs) and magnesium oxide nanoparticles (MgO-NPs), Saudi. J. Biol. Sci. 28 (2021) 5157—5167.

[18] K.A. Sukkar, A.A. Karamalluh, T.N. Jaber, Rheological and thermal properties of lubricating oil enhanced by the effect of CuO and TiO_2 nano-additives, Al-Khwarizmi Eng. J. 15 (2019) 24—33.

[19] Z. Sabouri, S. Sabouri, S.S. Tabrizi Hafez Moghaddas, A. Mostafapour, M.S. Amiri, M. Darroudi, Facile green synthesis of Ag-doped ZnO/CaO nanocomposites with Caccinia macranthera seed extract and assessment of their cytotoxicity, antibacterial, and photocatalytic activity, Bioproc. Biosyst. Eng. 45 (2022) 1799—1809.

[20] S. Vasantharaj, S. Sathiyavimal, P. Senthilkumar, V.N. Kalpana, G. Rajalakshmi, M. Alsehli, A. Elfasakhany, A. Pugazhendhi, Enhanced photocatalytic degradation of water pollutants using bio-green synthesis of zinc oxide nanoparticles (ZnO NPs), J. Environ. Chem. Eng. 9 (2021) 105772.

[21] S.T. Bunyan, A.A.-K.M. Hasan, Experimental study of the influence of nanoparticles additive to diesel fuel on the emission characteristics, Al-Khwarizmi Eng. J. 17 (2021) 13—19.

[22] T. Sen, S. Mishra, N.G. Shimpi, A b -cyclodextrin based binary dopant for polyaniline : structural , thermal , electrical , and sensing performance, Mater. Sci. Eng. B. 220 (2017) 13—21.

[23] Y.A. Mustafa, A.I. Alwared, M. Ebrahim, Heterogeneous photocatalytic degradation for treatment of oil from wastewater, Al-Khwarizmi Eng. J. 10 (2014) 53—61.

[24] S.J. Charde, S.S. Sonawane, A.P. Rathod, S.H. Sonawane, N.G. Shimpi, V.R. Parate, Copper-Doped zinc oxide nanoparticles : influence on thermal , thermo mechanical, and Tribological Properties of Polycarbonate, 2017, pp. 1—9, 10.

[25] A.M. Huerta-Flores, E. Luévano-Hipólito, L.M. Torres-Martínez, A. Torres-Sánchez, Photocatalytic H2 production and CO_2 reduction on Cu, Ni-doped ZnO: effect of metal doping and oxygen vacancies, J. Mater. Sci. Mater. Electron. 30 (2019) 18506—18518.

[26] X. Liu, L. Ye, S. Liu, Y. Li, X. Ji, Photocatalytic reduction of CO2 by ZnO micro/nanomaterials with different morphologies and ratios of {0001} facets, Sci. Rep. 6 (2016) 1—9.

[27] M. Fazlzadeh, K. Rahmani, A. Zarei, H. Abdoallahzadeh, F. Nasiri, R. Khosravi, A novel green synthesis of zero valent iron nanoparticles (NZVI) using three plant extracts and their efficient application for removal of Cr(VI) from aqueous solutions, Adv. Powder Technol. 28 (2017) 122—130.

[28] S. Chowdhury, R. Balasubramanian, Graphene/semiconductor nanocomposites (GSNs) for heterogeneous photocatalytic decolorization of wastewaters contaminated with synthetic dyes: a review, Appl. Catal. B Environ. 160—161 (2014) 307—324.

[29] L.V. Bora, R.K. Mewada, Visible/solar light active photocatalysts for organic effluent treatment: fundamentals, mechanisms and parametric review, Renew. Sustain. Energy Rev. 76 (2017) 1393—1421.

[30] A. Bouafia, S. Meneceur, S. Chami, S.E. Laouini, H. Daoudi, S. Legmairi, H.A. Mohammed Mohammed, N. Aoun, F. Menaa, Removal of hydrocarbons and heavy metals from petroleum water by modern green nanotechnology methods, Sci. Rep. 13 (2023) 5637.

[31] M. Imran, H. Jan, S. Faisal, S. Ali Shah, S. Shah, M. Naeem Khan, M. Taj Akbar, M. Rizwan, F. Jan, S. Syed, In vitro examination of anti-parasitic, anti-Alzheimer, insecticidal and cytotoxic potential of Ajuga bracteosa Wallich leaves extracts, Saudi J. Biol. Sci. 28 (2021) 3031—3036.

[32] M. Ahmad, W. Rehman, M.M. Khan, M.T. Qureshi, A. Gul, S. Haq, R. Ullah, A. Rab, F. Menaa, Phytogenic fabrication of

ZnO and gold decorated ZnO nanoparticles for photocatalytic degradation of Rhodamine B, J. Environ. Chem. Eng. 9 (2021) 104725.

[33] N.G. Shimpi, J. Verma, S. Mishra, Preparation, characterization and properties of poly(vinyl chloride)/CaSO4 nanocomposites, Polym. - Plast. Technol. Eng. 48 (2009) 997–1001.

[34] B. Uzair, A. Liaqat, H. Iqbal, B. Menaa, A. Razzaq, G. Thiripuranathar, N.F. Rana, F. Menaa, Green and cost-effective synthesis of metallic nanoparticles by algae: safe methods for translational medicine, Bioengineering 7 (2020) 1–22.

[35] A.D. Mali, N.G. Shimpi, S. Mishra, Thermal, mechanical and morphological properties of surface-modified montmorillonite-reinforced Viton rubber nanocomposites, Polym. Int. 63 (2014) 338–346.

[36] U. Wijesinghe, G. Thiripuranathar, H. Iqbal, F. Menaa, Biomimetic synthesis, characterization, and evaluation of fluorescence resonance energy transfer, photoluminescence, and photocatalytic activity of zinc oxide nanoparticles, Sustain 13 (2021) 1–22.

[37] J. Santhoshkumar, S.V. Kumar, S. Rajeshkumar, Synthesis of zinc oxide nanoparticles using plant leaf extract against urinary tract infection pathogen, Resour. Technol. 3 (2017) 459–465.

[38] M. Khan, P. Ware, N. Shimpi, Synthesis of ZnO nanoparticles using peels of Passiflora foetida and study of its activity as an efficient catalyst for the degradation of hazardous organic dye, SN Appl. Sci. 3 (2021) 1–17.

[39] B. Gherbi, S.E. Laouini, S. Meneceur, A. Bouafia, H. Hemmami, M.L. Tedjani, G. Thiripuranathar, A. Barhoum, F. Menaa, Effect of pH value on the bandgap energy and particles size for biosynthesis of ZnO nanoparticles: efficiency for photocatalytic adsorption of methyl orange, Sustain 14 (2022) 11300.

[40] S.S. Ahmed, A.M. Alqahtani, T. Alqahtani, A.H. Alamri, F. Menaa, R.K. Mani, B.D. R, K. Kavitha, Green synthesis, characterizations of zinc oxide nanoparticles from aqueous leaf extract of Tridax procumbens Linn. And assessment of their anti-hyperglycemic activity in streptozoticin-induced diabetic rats, Materials 15 (2022) 8202.

[41] S. Khanam, S.K. Rout, A photocatalytic hydrolysis and degradation of toxic dyes by using plasmonic metal–semiconductor heterostructures: a review, Chem 4 (2022) 454–479.

[42] A.K. Hassan, M.A. Atiya, Z.A. Mahmoud, Photo-Fenton-like degradation of direct blue 15 using fixed bed reactor containing bimetallic nanoparticles: effects and Box–Behnken optimization, Environ. Technol. Innov. 28 (2022) 102907.

[43] X. Weng, Z. Chen, Z. Chen, M. Megharaj, R. Naidu, Clay supported bimetallic Fe/Ni nanoparticles used for reductive degradation of amoxicillin in aqueous solution: characterization and kinetics, Coll. Surf. A Physicochem. Eng. Asp. 443 (2014) 404–409.

[44] M.S. Khan, P.P. Dhavan, B.L. Jadhav, N.G. Shimpi, Ultrasound-Assisted green synthesis of Ag-decorated ZnO nanoparticles UsingExcoecaria agallochaLeaf extract and evaluation of their photocatalytic and biological Activity, 2020, pp. 12660–12671, 5.

[45] A.P. Shah, S. Jain, N.G. Shimpi, Enhanced photocatalytic activity of electrospun PAN/Ag-G NFs under solar irradiation for effective degradation of hazardous organic dyes, Chem. Select 5 (2020) 3897–3905.

[46] K. Sravanthi, D. Ayodhya, P.Y. Swamy, Green synthesis, characterization and catalytic activity of 4-nitrophenol reduction and formation of benzimidazoles using bentonite supported zero valent iron nanoparticles, Mater. Sci. Energy Technol. 2 (2019) 298–307.

[47] A.P. Shah, A.S. Sharma, V.S. Sharma, N. Shimpi, Polyacrylonitrile nanofibers incorporating Ag-decorated graphitic carbon nitride for the visible-light-activated selective oxidation of styrene , benzylic methylene groups , and benzene polyacrylonitrile nanofibers incorporating Ag-decorated

graphitic carbon nitride for the visible-light-activated selective oxidation of styrene, Benzylic Methyl. Groups Benz. 3 (2019) 1922–1933.

[48] R. Ullah, S. Shah, Z. Muhammad, S.A. Shah, S. Faisal, U. Khattak, T. Ul Haq, M.T. Akbar, In vitro and in vivo applications of Euphorbia wallichii shoot extract-mediated gold nanospheres, Green Process. Synth. 10 (2021) 101–111.

[49] S. Jain, N. Karmakar, A. Shah, N.G. Shimpi, Development of Ni doped ZnO/polyaniline nanocomposites as high response room temperature NO2 sensor, Mater. Sci. Eng. B Solid-State Mater. Adv. Technol. 247 (2019) 114381.

[50] M.S. Khan, P.P. Dhavan, B.L. Jadhav, N.G. Shimpi, Ultrasound-Assisted green synthesis of Ag-decorated ZnO nanoparticles UsingExcoecaria agallochaLeaf extract and evaluation of their photocatalytic and biological activity, 2020, pp. 12660–12671, 5.

[51] M. Imran, H. Jan, S. Faisal, S. Ali Shah, S. Shah, M. Naeem Khan, M. Taj Akbar, M. Rizwan, F. Jan, S. Syed, In vitro examination of anti-parasitic, anti-Alzheimer, insecticidal and cytotoxic potential of Ajuga bracteosa Wallich leaves extracts, Saudi J. Biol. Sci. 28 (2021) 3031–3036.

[52] T. Sen, N.G. Shimpi, S. Mishra, R. Sharma, Polyaniline/γ-Fe2O3 nanocomposite for room temperature LPG sensing, Sens. Actuat. B Chem. 190 (2013) 120–126.

[53] S. Pai, S, H, T. Varadavenkatesan, R. Vinayagam, R. Selvaraj, Photocatalytic zinc oxide nanoparticles synthesis using Peltophorum pterocarpum leaf extract and their characterization, Optik (Stuttg) 185 (2019) 248–255.

[54] S. Mishra, N.G. Shimpi, Mechanical and flame-retarding properties of styrene – butadiene rubber filled with nano-CaCO₃ as a filler and linseed Oil as an Extender, 2005, pp. 2563–2571, 6.

[55] A.T. Mansour, A.E. Alprol, M. Khedawy, K.M. Abualnaja, T.A. Shalaby, G. Rayan, K.M.A. Ramadan, M. Ashour, Green synthesis of zinc oxide nanoparticles using red seaweed for the elimination of organic toxic dye from an aqueous solution, Materials 15 (2022) 1–25.

[56] J. Khan, M. Tariq, M. Muhammad, M.H. Mehmood, I. Ullah, A. Raziq, F. Akbar, M. Saqib, A. Rahim, A. Niaz, Kinetic and thermodynamic study of oxidative degradation of acid yellow 17 dye by Fenton-like process: effect of HCO3−, CO32−, Cl− and SO42− on dye degradation, Bull. Chem. Soc. Ethiop. 33 (2019) 243–254.

[57] A.R. Puthukkara P, S. Jose T, D. lal S, Plant mediated synthesis of zero valent iron nanoparticles and its application in water treatment, J. Environ. Chem. Eng. 9 (2021) 104569.

[58] R.P. Singh, V.K. Shukla, R.S. Yadav, P.K. Sharma, P.K. Singh, A.C. Pandey, Biological approach of zinc oxide nanoparticles formation and its characterization, Adv. Mater. Lett. 2 (2011) 313–317.

[59] A.S. Mahmoud, A. Ismail, M.K. Mostafa, M.S. Mahmoud, W. Ali, A.M. Shawky, Isotherm and kinetic studies for heptachlor removal from aqueous solution using Fe/Cu nanoparticles, artificial intelligence, and regression analysis, Sep. Sci. Technol. 55 (2020) 684–696.

[60] L. Chen, J. Tian, H. Qiu, Y. Yin, X. Wang, J. Dai, P. Wu, A. Wang, L. Chu, Preparation of TiO2 nanofilm via sol-gel process and its photocatalytic activity for degradation of methyl orange, Ceram. Int. 35 (2009) 3275–3280.

[61] S. Mishra, N.G. Shimpi, U.D. Patil, Effect of nano CaCO3 on thermal properties of styrene Butad. Rubber (SBR), 2007, pp. 449–459, 14.

[62] S. Azizi, M.M. Shahri, R. Mohamad, Green synthesis of zinc oxide nanoparticles for enhanced adsorption of lead Ions from aqueous solutions: equilibrium, kinetic and thermodynamic studies, Molecules 22 (2017) 831.

[63] M. kermani, A. Mostafapour, Sabouri, Z. Darroudi, The photocatalytic, cytotoxicity, and antibacterial properties of zinc oxide nanoparticles synthesized using Trigonella foenum-graecum L extract, Environ. Sci. Pollut. Res. 30 (2023) 19313–19325.

[64] W.J. Fendi, J.A. Naser, Adsorption isotherms study of methylene blue dye on membranes from electrospun nanofibers, orient, J. Chem. 34 (2018) 2884–2894.

[65] V. C, M.N.C. Prabha, M.A.L.A. Raj, Green mediated synthesis of zinc oxide nanoparticles for the photocatalytic degradation of Rose Bengal dye, Environ. Nanotechnol. Monit. Manag. 6 (2016) 134–138.

[66] M.N. Zafar, Q. Dar, F. Nawaz, M.N. Zafar, M. Iqbal, M.F. Nazar, Effective adsorptive removal of azo dyes over spherical ZnO nanoparticles, J. Mater. Res. Technol. 8 (2019) 713–725.

[67] P. Ma, Q. Liu, P. Liu, H. Li, X. Han, L. Liu, W. Zou, Green synthesis of Fe/Cu oxides composite particles stabilized by pine needle extract and investigation of their adsorption activity for norfloxacin and ofloxacin, J. Dispers. Sci. Technol. 42 (2021) 1350–1367.

[68] S. Malaysiana, S. Hijau, N. Nikel, P. Pewarna, Green synthesis of nickle oxide nanoparticles for adsorption of Dyes, 2022, pp. 533–546, 51.

[69] G.K. Weldegebrieal, Synthesis method, antibacterial and photocatalytic activity of ZnO nanoparticles for azo dyes in wastewater treatment: a review, Inorg. Chem. Commun. 120 (2020) 108140.

[70] Q. Hu, S. Pang, D. Wang, In-depth insights into mathematical characteristics, selection criteria and common mistakes of adsorption kinetic models: a critical review, Sep. Purif. Rev. 51 (2022) 281–299.

[71] F.C. Wu, R.L. Tseng, R.S. Juang, Characteristics of Elovich equation used for the analysis of adsorption kinetics in dye-chitosan systems, Chem. Eng. J. 150 (2009) 366–373.

[72] S. Raghav, D. Kumar, Adsorption equilibrium, kinetics, and thermodynamic studies of fluoride adsorbed by tetrametallic oxide adsorbent, J. Chem. Eng. Data. 63 (2018) 1682–1697.

[73] A.A. Mohammed, T.J. Al-Musawi, S.L. Kareem, M. Zarrabi, A.M. Al-Ma'abreh, Simultaneous adsorption of tetracycline, amoxicillin, and ciprofloxacin by pistachio shell powder coated with zinc oxide nanoparticles, Arab. J. Chem. 13 (2020) 4629–4643.

[74] A.K. Dey, A. Dey, R. Goswami, Adsorption characteristics of methyl red dye by Na2CO3-treated jute fibre using multi-criteria decision making approach, Appl. Water Sci. 12 (2022) 1–22.

[75] K.M. Al-Qahtani, Cadmium removal from aqueous solution by green synthesis zero valent silver nanoparticles with Benjamina leaves extract, Egypt, J. Aquat. Res. 43 (2017) 269–274.

[76] R. Yuvakkumar, J. Suresh, B. Saravanakumar, A. Joseph Nathanael, S.I. Hong, V. Rajendran, Rambutan peels promoted biomimetic synthesis of bioinspired zinc oxide nanochains for biomedical applications, Spectr. Acta Part A Mol. Biomol. Spectrosc. 137 (2015) 250–258.

[77] D. Dodoo-Arhin, T. Asiedu, B. Agyei-Tuffour, E. Nyankson, D. Obada, J.M. Mwabora, Photocatalytic degradation of Rhodamine dyes using zinc oxide nanoparticles, Mater, Today Proc. 38 (2021) 809–815.

[78] G.F. Khaleel, I. Ismail, A.H. Abbar, Heliyon Application of solar photo-electro-Fenton technology to petroleum refinery wastewater degradation : optimization of operational parameters, Heliyon 9 (2023) e15062.

[79] H. Sawalha, R. Abiri, R. Sanusi, N.A. Shaharuddin, A.A.M. Noor, N.A.A. Shukor, H. Abdul-Hamid, S.A. Ahmad, Toward a better understanding of metal nanoparticles, a novel strategy from eucalyptus plants, Plants 10 (2021) 1–22.